



Absolute configuration and biological profile of pyrazoline enantiomers as MAO inhibitory activity

Umut Salgin Goksen^{1,2} | Sevgi Sarigul³ | Patrick Bultinck⁴ | Wouter Herrebout⁵ |
Ilknur Dogan³ | Kemal Yelekci⁶ | Gulberk Ucar⁷ | Nesrin Gokhan Kelekci¹

¹Department of Pharmaceutical Chemistry, Faculty of Pharmacy, Hacettepe University, Ankara, Turkey

²Analyses and Control Laboratories, Turkish Medicines and Medical Devices Agency, Ankara, Turkey

³Chemistry Department, Boğaziçi University, Istanbul, Turkey

⁴Department of Chemistry, Ghent University, Ghent, Belgium

⁵Department of Chemistry, University of Antwerp, Antwerp, Belgium

⁶Department of Bioinformatics and Genetics, Faculty of Engineering and Natural Sciences, Kadir Has University, Istanbul, Turkey

⁷Department of Biochemistry, Faculty of Pharmacy, Hacettepe University, Ankara, Turkey

Correspondence

Nesrin Gokhan Kelekci, Department of Pharmaceutical Chemistry, Faculty of Pharmacy, Hacettepe University, 06100, Sıhhiye, Ankara, Turkey.
Emails: onesrin@gmail.com; onesrin@hacettepe.edu.tr

Funding information

Hacettepe University Scientific Research Projects Coordination Unit, Grant/Award Numbers: 1527 and 012D06301001; IOF; BOF; FWO-Vlaanderen; Scientific and Technological Research Council of Turkey, Grant/Award Number: 112T746

Abstract

A new racemic pyrazoline derivative was synthesized and resolved to its enantiomers using analytic and semipreparative high-pressure liquid chromatography. The absolute configuration of both fractions was established using vibrational circular dichroism. The in vitro monoamine oxidase (MAO) inhibitory profiles were evaluated for the racemate and both enantiomers separately for the two isoforms of the enzyme. The racemic compound and both enantiomers were found to inhibit hMAO-A selectively and competitively. In particular, the *R* enantiomer was detected as an exceptionally potent and a selective MAO-A inhibitor ($K_i = 0.85 \times 10^{-3} \pm 0.05 \times 10^{-3} \mu\text{M}$ and $\text{SI}: 2.35 \times 10^{-5}$), whereas *S* was determined as poorer compound than *R* in terms of K_i and SI (0.184 ± 0.007 and 0.001). The selectivity of the enantiomers was explained by molecular modeling docking studies based on the PDB enzymatic models of MAO isoforms.

KEYWORDS

2-pyrazoline, molecular modeling docking, monoamine oxidase inhibitory activity, specific rotation, stereochemistry, vibrational circular dichroism

1 | INTRODUCTION

Monoamine oxidase (MAO) is a flavin adenine dinucleotide (FAD)-containing enzyme that is located in the outer mitochondrial membranes of neuronal, glial, and other cells.^{1,2} It catalyzes the oxidative deamination of biogenic

amines in the brain³ and the peripheral tissues, regulating their level.⁴ Monoamine oxidase exists in two forms, MAO-A and MAO-B.⁴ Monoamine oxidase-A catalyzes the oxidative deamination of serotonin (5-HT), adrenaline (A), and noradrenaline (NA) and is selectively inhibited by the irreversible inhibitor clorgyline and the

reversible inhibitor moclobemide. Monoamine oxidase-B catalyzes the oxidative deamination of phenylethylamine and benzylamine and is selectively inhibited by the irreversible inhibitor selegiline.^{4,5}

Monoamine oxidase-A and MAO-B play essential roles in vital physiological processes and are involved in the pathogenesis of various diseases in human.^{6,7} Due to their key role, MAO inhibitors represent a useful tool for the treatment of several psychiatric and neurological diseases. In particular, reversible and selective MAO-A inhibitors are used as antidepressant and anti-anxiety drugs, while MAO-B inhibitors have been found to be useful as adjuvants in the treatment of Parkinson's disease and Alzheimer's disease (AD).⁸⁻¹⁵

The development of MAO inhibitors started with hydrazine derivatives. However, they were withdrawn due to their toxic side effects.¹⁶ Subsequently, different families of heterocycles containing 2 or 4 nitrogen atoms were used as scaffolds for synthesizing reversible and selective MAO inhibitors.¹⁷⁻²³ 2-Pyrazolines, which form one of these families, can also be considered as a cyclic hydrazine derivative. On the basis of the clinical profiles of hydrazine and other heterocycles, researchers focused on structural modifications of the pyrazoline to enhance the pharmacological activity. Various pyrazoline derivatives were synthesized and screened for their MAO, bovine serum amine oxidase, and semicarbazide sensitive amine oxidase activities. A considerable number of the prepared compounds were found to have bovine serum amine oxidase, semicarbazide sensitive amine oxidase, and MAO inhibitory activities comparable with or higher than the reference compounds.²⁴⁻³⁴

In the light of the aforementioned findings and continuing our study of pyrazoline derivatives as potential inhibitors of MAO-A and MAO-B isoforms, we synthesized a series of 30 new pyrazoline derivatives that possess a stereogenic center on the 5 position of the ring and 9 new hydrazone derivatives. New compounds were screened for their *in vitro* hMAO inhibitory activities using recombinant hMAO isoforms. All compounds inhibited hMAO-A potently, selectively, and reversibly. Five compounds of these series exhibiting highest inhibitory potency and selectivity toward hMAO-A were assessed for acute and subchronic antidepressant effects using Porsolt's forced swimming test on mice. Our data elicited that they have an antidepressant-like action in mice by possibly interacting with the monoaminergic and serotonergic system (Umut Salgın Gökşen, unpublished results).

Then, we decided to do semipreparative chromatographic enantioseparation of the most potent and selective compound and to see the effect of the enantiomers on the MAO activity. We established the absolute

configuration using VCD. To this end the *R* and *S* enantiomers of the biologically active 1-[2-(2-benzoxazolinone-3-yl)acetyl]-3-phenyl-5-(3,4-dimethoxyphenyl)-4,5-dihydro-(1*H*)-pyrazole resolved on a chiral stationary phase were also submitted to *in vitro* biological evaluation. The results revealed that the *R*-enantiomer shows higher MAO-A inhibitory activity than the *S*-enantiomer.

2 | MATERIALS AND METHODS

2.1 | General information

All chemicals and solvents used were purchased from Merck A.G. and Aldrich Chemical Co. The melting point of the new compound **5** was determined using a Thomas Hoover Capillary Melting Point Apparatus. The specific rotations of the enantiomers dissolved in acetone were determined using a Polarimeter Rudolph Autopol IV at 25°C operating at the sodium D line. The infrared (IR) spectra were obtained using a Perkin Elmer Spectrum One and a Nicolet 520 FTIR spectrometer. ¹H-NMR spectra in dimethylsulfoxide (DMSO-*d*₆) were recorded on a Bruker 400-MHz UltraShield spectrometer. Electron impact mass spectrometry of the sample in methanol was performed using a Waters 2695 Alliance Micromass ZQ LC/MS spectrometer. Elemental analysis (C, H, N) was performed using a LECO CHNS 932 analyzer. The purity of the compound was assessed by TLC on silicagel HF₂₅₄ + 366.

3 | SYNTHESIS AND STRUCTURAL ELUCIDATION

2-Benzoxazolinone (**1**), ethyl (2-benzoxazolinone-3-yl)acetate (**2**), and 2-(2-benzoxazolinone-3-yl)acetylhydrazine (**3**) were synthesized according to previous methods.³⁵⁻³⁷

3.1 | 1-Phenyl-3-(3,4-dimethoxyphenyl)-2-propen-1-one (**4**) (chalcone)

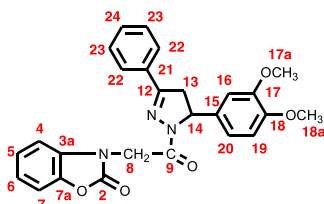
Preparation of **4** was done according to a previously described method,³⁸ providing the chalcone (2.36 g, 88%). mp 86.5–88.5°C (from ethanol : water [3:1]) (lit., 88°C^{39,40}).

3.2 | 1-[2-(2-Benzoxazolinone-3-yl)acetyl]-3-phenyl-5-(3,4-dimethoxyphenyl)-4,5-dihydro-(1*H*)-pyrazole (**5**)

2-(2-Benzoxazolinone-3-yl)acetylhydrazine **3** (1 mmol) was dissolved in 2 mL of DMF and 20 mL of *n*-propanol. Chalcone **4** (1 mmol) and eight drops of hydrochloric acid

were added to this solution and the latter refluxed for approximately 120 hours.⁴¹ The reaction mixture was then cooled, and the precipitate was recrystallized to give the 4,5-dihydro-(1*H*)-pyrazole (0.18 g, 13%) as a white crystal. mp 204–204.5°C (from acetone : water [3:1]).

The purity of the synthesized compound was checked by elemental analysis. Its structure was determined using a combination of IR, ¹H-NMR, ¹³C-NMR, and ESI-MS. Both enantiomers exhibited identical IR, ¹H-NMR, ¹³C-NMR, and mass spectra.



The IR, ¹H-NMR, ¹³C-NMR, and mass spectral data are found to be IR V_{\max}/cm^{-1} : 3,069, 3,000, 2,944, 2,839 (C–H), 1,769, 1,680 (C=O), 1,603, 1,520, 1,490, 1,439 (C=C, C=N), 1,369, 1,237, 1,140, 1,020 (C–O–C, C–N); ¹H-NMR (400 MHz, DMSO-*d*₆) δ (ppm) J (Hz): 3.24 (1H, dd, H-13a, J_{AB} :18.3 Hz, J_{AX} :5.0 Hz), 3.716 (3H, s, H-17a), 3.722 (3H, s, H-18a), 3.91 (1H, dd, H-13b, J_{AB} :18.2 Hz, J_{BX} :11.7 Hz), 5.10 (1H, d, H-8a, J :17.6 Hz), 5.26 (1H, d, H-8b, J :17.6 Hz), 5.54 (1H, dd, H-14, J_{BX} :11.6 Hz, J_{AX} :5.0 Hz), 6.75 (1H, dd, H-20, J_1 :8.3 Hz, J_2 :1.9 Hz), 6.82 (1H, d, H-16, J :1.9 Hz), 6.89 (1H, d, H-19, J :8.4 Hz), 7.13 (1H, t, H-5), 7.19 (1H, t, H-6), 7.28 (1H, d, H-4, J_{45} :7.6 Hz), 7.36 (1H, d, H-7, J_{67} :7.7 Hz), 7.49–7.52 (3H, m, H-23 and H-24), 7.86–7.88 (2H, m, H-22); ¹³C-NMR (400 MHz, DMSO-*d*₆) δ (ppm): 42.0 (C-13), 43.8 (C-8), 55.4 (C-17a), 55.5 (C-18a), 59.9 (C-14), 109.4 (C-7), 109.5 (C-5 ve C-6), 111.9 (C-4), 117.3 (C-16), 122.2 (C-19), 123.8 (C-20), 126.9 (C-23), 128.7 (C-22), 130.61 (C-24), 130.65 (C-3a), 131.4 (C-21), 133.9 (C-15), 141.8 (C-7a), 148.0 (C-18), 148.8 (C-17), 154.0 (C-12), 156.0 (C-2), 163.1 (C-9); ESI-MS m/z : 496 ([M + K]⁺, 3%), 481 ([M + H + Na]⁺, %31), 480 ([M + Na]⁺, %100), 458 ([M + H]⁺, %17), 320 ([M⁺-C₆H₃(OCH₃)₂]⁺, %17), 176 ([2-benzoks.-CH₂-CO]⁺, %13), 148 (2-benzoks.-CH₂)⁺, %16). Found: C, 68.18; H, 5.06; N, 9.15. Calculated for C₂₆H₂₃N₃O₅: C, 68.26; H, 5.07; N, 9.19.

4 | ANALYTIC SEPARATION AND STEREOCHEMISTRY-HPLC ANALYSIS

Liquid chromatography was performed using an ultraviolet detector Shimadzu SPD-6A ($\lambda = 254$ nm) in combination with a CHIRALPAK AD-H column packed with amylose tris (3,5-dimethylphenylcarbamate) (the column

for the analyses had particle size 5 μm ; column size 250 \times 4.6 mm, the semipreparative column had particle size 5 μm ; column size 250 \times 10 mm) as stationary phase at 35°C. The chromatograms were recorded, and the chromatographic peaks were integrated using the Shimadzu C-R6A Chromatopac software.

5 | VIBRATIONAL CIRCULAR DICHROISM SPECTRA

The stereochemistry of the separate enantiomers was determined by vibrational circular dichroism (VCD). Infrared and VCD spectra of the compounds were obtained using a BioTools ChiralIR-2X dual PEM spectrometer. Solutions containing up to 3.0 mg of the samples from both fractions from the analytical separation were dissolved in CDCl₃. Spectra were recorded in a 100- μm liquid cell equipped with BaF₂ windows. For both enantiomers, 40,000 scans were recorded at 4-cm⁻¹ resolution and averaged. The analysis reported below is based on the experimental spectra of the first eluent. A virtual racemate was used for baseline subtraction. Hence, spectra for the two enantiomers are exact mirror images.

Extensive conformational analyses were performed using the MMFF94S,⁴² MMF,⁴³ and SYBYL⁴⁴ force fields using the Monte Carlo and reservoir-filling algorithms, as implemented in the Spartan08⁴⁵ and Conflex^{46,47} software packages, respectively. The geometries derived from the molecular mechanics simulations were optimized at the density functional theory level using Gaussian 09⁴⁸ using the B3LYP/6-31G* and B3LYP/cc-pVTZ combinations of density functional theory functional and basis set and a SCRF model to account for solvent interactions. Boltzmann weighted IR and VCD spectra were obtained by assuming Lorentzian band profiles with a FWHH of 10 cm⁻¹. The Boltzmann populations used were based on the standard enthalpies obtained. Inspection of the data shows that enlarging the basis set from 6-31G* to cc-pVTZ only has a minor influence on the IR and VCD spectra. Both the experimental and theoretical spectra are shown in Figure 1.

6 | BIOCHEMISTRY

6.1 | Material

Recombinant hMAOs and other chemicals were purchased from Sigma-Aldrich. The Amplex[®]-Red MAO assay kit was obtained from Molecular Probes (Invitrogen Detection Technologies), USA.

Small amounts of compounds (approximately 5 mg) were used to prepare the stock solutions, and several dilutions obtained from these stocks were used in tests.

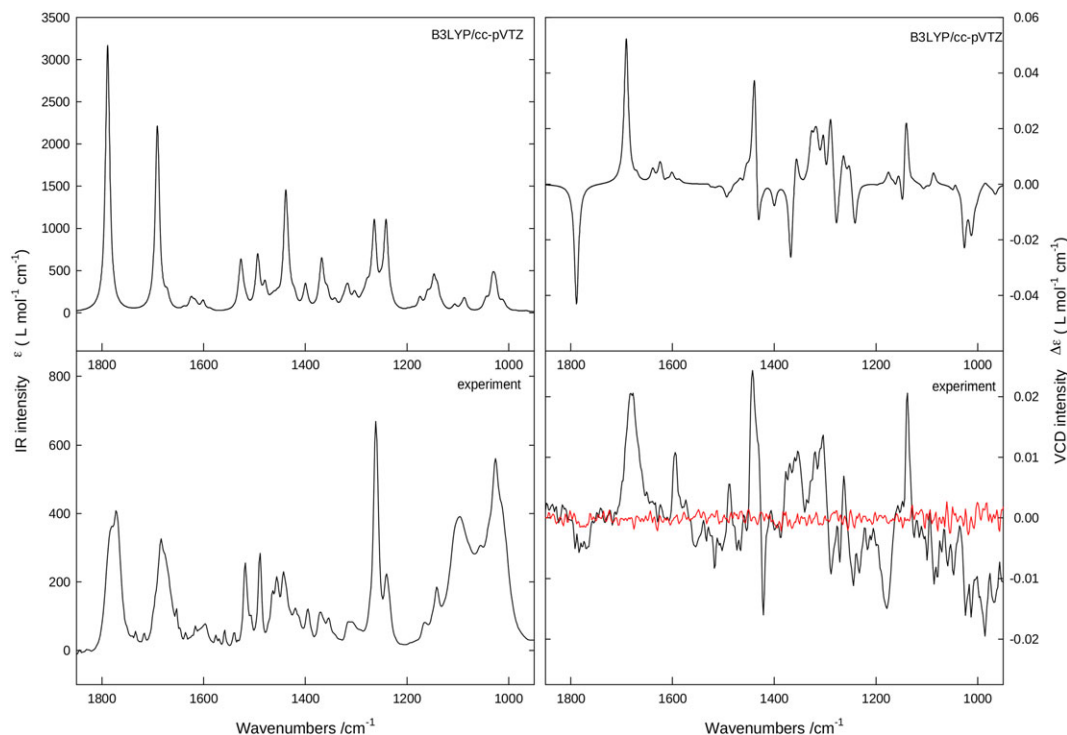


FIGURE 1 Experimental and calculated infrared and vibrational circular dichroism (VCD) spectra obtained for the **R** enantiomer of 1-[2-(2-benzoxazolinone-3-yl)acetyl]-3-phenyl-5-(3,4-dimethoxyphenyl)-4,5-dihydro-1*H*-pyrazole. For the experimental VCD spectra, the noise was added as a solid line in red. Due to the use of a virtual racemate for baseline subtractions, the experimental spectra for the R and S enantiomers are perfect mirror images

6.2 | Determination of MAO activity

The Amplex[®] Red MAO Assay Kit provides a one-step fluorometric method for the continuous measurement of MAO activity using a fluorescence microplate reader.^{49,50} The assay is based on the detection of H₂O₂ in a horse radish peroxidase coupled reaction using the Amplex Red reagent, a highly sensitive and stable probe for H₂O₂. Because resorufin, the reaction product, has absorption and fluorescence emission maxima of 571 and 585 nm, respectively, there is no significant interference from auto fluorescence.

Recombinant enzymes were diluted in a reaction buffer (containing 0.25 M of sodium phosphate, pH 7.4). One hundred microliters of hMAO-A or MAO-B solution was incubated with 0.2 μ L of inhibitor stock solution (clorgyline or pargyline, 0.5 mM) at room temperature for 30 minutes. Enzyme and inhibitor concentrations were kept as twofold lower in the final reaction volume. The positive control solution was prepared by diluting the 20-mM H₂O₂ working solution to the final concentration of 10 μ M in the reaction buffer, whereas the reaction buffer without H₂O₂ was prepared as the negative control. The reaction was started by adding 100 μ L of the Amplex Red reagent to each microplate well containing the samples and controls. The mixtures were incubated for 30 minutes at room temperature. The fluorescence was measured using excitation at 530 nm and emission at 590 nm at multiple

time points to follow the kinetics of the reactions. Background fluorescence was corrected by subtracting the values derived from the control (no enzyme). The possible capacity of the new compounds to modify the fluorescence generated in the reaction mixture due to nonenzymatic inhibition was determined by adding these compounds to solutions containing only the Amplex Red reagent in a sodium phosphate buffer. The newly synthesized compounds were tested for their possible interactions with Amplex Red reagent according to the method previously described,⁴⁹⁻⁵¹ and it was found that our compounds did not directly react with Amplex Red reagent.

6.3 | Kinetic studies

The synthesized derivatives were dissolved in dimethyl sulfoxide (DMSO), with a maximum concentration of 1% and used in a wide concentration range of 0.10 to 200.00 μ M. The reference inhibitors were also dissolved in DMSO in a concentration range of 0.001 to 20.00 μ M. The mode of MAO inhibition was examined using Lineweaver-Burk plotting. The slopes of the Lineweaver-Burk plots were plotted versus the inhibitor concentration, and the K_i values were determined from the x -axis intercept as $-K_i$. Each K_i value is the representative of single determination where the correlation coefficient (R^2) of the replotted

the slopes versus the inhibitor concentrations was at least 0.98. The selectivity index (SI) was calculated as K_i (hMAO-A)/ K_i (hMAO-B). The protein concentration was determined according to the Bradford method.⁵²

6.4 | Reversibility studies

The reversibility of the hMAO inhibition with the new compounds was determined by dialysis as previously described.⁵³ Dialysis tubing 16 × 25 mm (SIGMA) with a molecular weight cut-off of 12,000 Da and a sample capacity of 0.5 to 10 mL was used. Adequate amounts of the recombinant enzymes (hMAO-A or B; 1 U/mL) and the inhibitors at a concentration equal to fourfold the IC₅₀ values for the inhibition of hMAO-A and hMAO-B were incubated in a potassium phosphate buffer (0.05 M, pH 7.4, 5% sucrose containing 1% DMSO) for 15 minutes at 37°C. Another set was prepared by preincubation of the same amount of hMAO-A and hMAO-B with the reference inhibitors. The enzyme-inhibitor mixtures were subsequently dialyzed at 4°C in 80 mL of the dialysis buffer (100-mM potassium phosphate, pH 7.4, 5% sucrose). The dialysis buffer was replaced with fresh buffer twice during the 24 hours of dialysis. After dialysis, residual MAO activities were measured and expressed as mean ± SEM. For comparison, undialyzed mixtures of the MAOs and the inhibitors were included in the study.

6.5 | Cytotoxicity studies

The cell viability was determined by a MTT assay.⁵⁴ Human hepatoma cell line HepG2 (Invitrogen) was used. The cells were exposed to **5R** and **5S** at the concentrations of 1, 5, and 25 μM, and 0.1% DMSO as a vehicle control for 24 hours. Control cells treated with 0.1% DMSO were used as 100% viability.⁵⁵ Results were expressed as mean ± SEM. Differences are considered statistically significant at $P < .05$.

7 | MOLECULAR MODELING STUDIES

The crystal structures of MAO-A and MAO-B were extracted from the PDB (<http://www.rcsb.org>, for MAO-A pdb code: 2Z5X; human MAO in complex with harmine, resolution 2.2 Å⁵⁶ and for MAO-B pdb code: 2V5Z; human MAO-B in complex with inhibitor safinamide, resolution 1.6 Å⁵⁷). Each structure was cleaned of all water molecules and inhibitors as well as all noninteracting ions before being used in the docking studies. The initial oxidized form of the FAD was used in all docking studies. For MAO-A and MAO-B, one of the two subunits was taken

as the target structure. Using a fast Dreiding-like force field,⁵⁸ each protein's geometry was first optimized and then submitted to the "Clean Geometry" toolkit of the Discovery Studio (Accelrys, Inc.) for a more complete check. Missing hydrogen atoms were added based on the protonation state of the titratable residues at a pH of 7.4. The ionic strength was set to 0.145, and the dielectric constant was set to 10. The AutoDock Tools (vv. 1.5.4)⁵⁹ graphical user interface program was employed to setup the enzymes for molecular docking.

The 3D structures of the ligand molecules were built, optimized at PM3 level, and saved in pdb format. The AutoDock Tools package was also employed to generate the docking input files of the ligands. AutoDock 4.2.6 was used for all dockings; the detailed docking procedure has been given elsewhere,⁶⁰ and the detailed procedure was reported in our earlier work.⁶¹

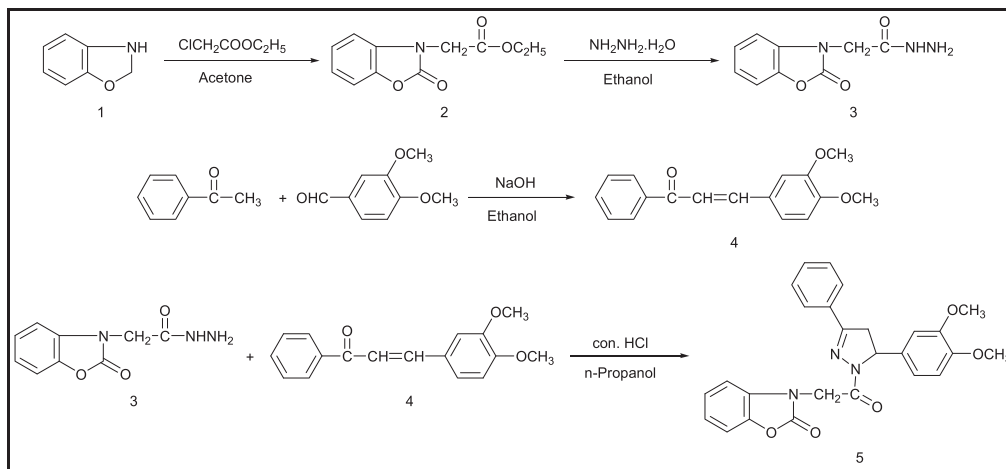
8 | RESULTS AND DISCUSSION

8.1 | Synthesis and characterization

The synthesis pathway of 1-[2-(2-benzoxazolinone-3-yl)acetyl]-3-phenyl-5-(3,4-dimethoxyphenyl)-4,5-dihydro-1H-pyrazole is given in Scheme 1. Treatment of 2-benzoxazolinone **1** with ethyl chloroacetate in K₂CO₃/acetone gave the *N*-alkylated product ethyl (2-benzoxazolinone-3-yl) acetate **2**.³⁵ The acid hydrazide **3** was prepared by the reaction of ethyl (2-benzoxazolinone-3-yl) acetate and hydrazine hydrate in ethanol.^{36,37} On the other hand, α,β-unsaturated carbonyl compound (chalcone) **4** was prepared by reacting 3,4-dimethoxybenzaldehyde and acetophenone under basic condition according to the Claisen-Schmidt condensation.³⁸ The reaction of hydrazide **3** with chalcone **4** in *n*-propanol under acidic condition gave compound 1-[2-(2-benzoxazolinone-3-yl)acetyl]-3-phenyl-5-(3,4-dimethoxyphenyl)-4,5-dihydro-1H-pyrazole **5** (Scheme 1).

Both enantiomers exhibited identical IR, ¹H-NMR, ¹³C-NMR, and mass spectra. The IR spectrum of **5** revealed two stretching bands at 1,769 and 1,680 cm⁻¹ due to the carbonyl function of the lactam and acetyl groups, respectively. C=C, C=N, and C—O—C, C—N stretching bands were found near 1,603 to 1,439 cm⁻¹ and 1,369 to 1,020 cm⁻¹, respectively. The existence of the C=N stretching bands and disappearance of the N—H stretching bands prove the closure of the 4,5-dihydro-(1H)-pyrazole ring. Aromatic and aliphatic C—H stretching bands were observed near 3,069 to 2,839 cm⁻¹.

In the ¹H-NMR spectrum of **5**, multiplet or doublet peaks belonging to the protons of aromatic rings were observed at 7.88 to 6.75 ppm. Three distinct doublet of



SCHEME 1 Synthesis pathway of 1-[2-(2-benzoxazolinone-3-yl)acetyl]-3-phenyl-5-(3,4-dimethoxyphenyl)-4,5-dihydro-1H-pyrazole 5

doublets of the ABX system in the 4,5-dihydro-(1H)-pyrazole ring (a CH proton and two anisochronous protons of a CH₂) appeared at 5.54 to 3.24 ppm. The CH (H_x) proton appeared at 5.54 ppm due to vicinal coupling with the two magnetically nonequivalent protons of the methylene group at position 4 of the 4,5-dihydro-(1H)-pyrazole ring. The signals of H_A and H_B of the 4,5-dihydro-(1H)-pyrazole ring were observed as doublet of doublets at 3.24 and 3.91 ppm, respectively. The CH₂ protons between the 2-benzoxazolinone and 4,5-dihydro-(1H)-pyrazole ring resonated as a pair of doublet of doublets at 5.10 and 5.26 ppm. The signals for methoxy groups appeared at 3.72 ppm as two separate peaks. Additional support for the structure of **5** was provided by ¹³C-NMR spectra. In the ¹³C-NMR spectra, the lactam and acetyl C=O groups gave two peaks at around 156 and 163 ppm. The peak at 154 ppm in the ¹³C-NMR spectrum assigned to the C=N moiety confirms the closure of 4,5-dihydro-(1H)-pyrazole ring). The ions produced under electrospray ionization showed a characteristic [M + Na]⁺ ion peak as the base signal in the mass spectrum.

8.2 | Analytic separation and absolute configuration

Because it is known that the two enantiomers of a chiral molecule may exhibit different biological activities,⁶²⁻⁶⁵ we have decided to separate both enantiomers to evaluate their separate selective human MAO inhibitory activities. This separation was achieved for both enantiomers of **5** using analytic and semipreparative HPLC. In this way, 5 mg of each enantiomer was resolved and used further in VCD and MAO inhibition studies.

During the separation, the compound was dissolved in methanol and 30 μL was injected to the column. The

choice of the eluent was done as follows: First, different ratios of hexane : ethanol mixtures were tried as the mobile phase; however, none of them could resolve the compound into its enantiomers. Therefore, it was decided to use a more polar mobile phase. When an ethanol : methanol mixture with 80:20 ratio was used, the resolution was again not achieved. The enantiomers were finally resolved analytically with the separation factor (α) of 1.36 when a 50:50 ethanol : methanol mixture was used as the eluent (flow rate 0.4 mL/min). The enantiomers were then collected by semipreparative HPLC using an CHIRALPAK AD-H semipreparative column under the same conditions. One hundred microliters of multiple injections of the racemate afforded pure enantiomers (Figure 2).

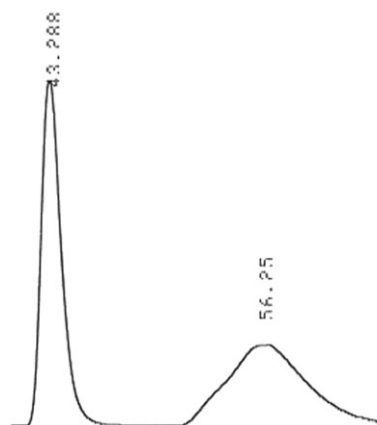


FIGURE 2 High-performance liquid chromatography chromatogram of **5** showing the first eluted (retention time 43.29 min) and the second eluted (retention time 56.25 min) enantiomer at 35°C. Column: Chiralpak AD-H, eluent (vol/vol) 50:50 ethanol : methanol flow rate: 0.4 mL/min (α):1.36

1. Eluent (R-enantiomer): $[\alpha]_{365}^{25} = +[25 \pm 3]$ (c 0.0008 g/mL in acetone).

8.3 | Eluent (S-enantiomer): $[\alpha]_{365}^{25} = -(25 \pm 3)$ (c 0.0009 g/mL in acetone)

The measurement of circular dichroism associated with molecular vibrational transitions is referred to as VCD.⁶⁶⁻⁶⁸ The assignment of the absolute configuration of the collected enantiomers was performed using VCD. The experimental IR and VCD spectra for the first eluent and the calculated IR and VCD spectra for the *R* enantiomer obtained at the B3LYP/cc-pVTZ level are shown in Figure 1. Due to the limited amount of sample available, the absorbances in IR are rather small and the corresponding VCD spectrum is characterized by a substantial noise level. However, in general, good agreement is found in which most, if not all, of the characteristic features observed are reproduced by the calculations. The agreement between experiment and theory allows the characterization of the absolute configuration of the first eluent as *R* and that of the second eluent as *S*.

Numerical data confirming the assignment of the absolute configuration of the first eluent as the *R* enantiomer and the second eluent as the *S* enantiomer were obtained using the CompareVOA algorithm described in Debie et al.⁶⁹ Enantiomers have exactly the same IR spectrum and hence the same similarity measure between the theoretical and experimental IR spectra. The B3LYP/cc-pVTZ IR similarity index, using a scaling factor for the calculated frequencies of 0.985, and based upon the 1,000 to 1,800 cm^{-1} spectral range studied, is determined to be 65.1%. Vibrational circular dichroism spectra, however, show a mirror image relationship between enantiomers. Using the experimental spectrum of the first eluent, we computed the similarity index between this experimental spectrum and the theoretical spectra of the *R* and *S* enantiomers. The similarity between this first experimental spectrum and the theoretical spectrum for a computed *R* enantiomer amounts 68.5%. The similarity between the first experimental spectrum and that for a computed *S* spectrum amounts only 19.6%. This leads to an enantiomeric similarity index of 48.9%. This establishes that the first eluent corresponds to the *R* enantiomer. The confidence level for the assignment, based on the localization of the current assignments with respect to the database of correct and incorrect assignments contained in the CompareVOA algorithm, is 99%. All calculations and analysis were repeated at the B3LYP/6-31G* level of theory and resulted in very similar results albeit slightly worse. Using the experimental spectrum of the second eluent, we

computed the similarity between this second experimental spectrum and the theoretical spectrum for a computed *R* enantiomer to be 19.6%. The similarity between this second experimental spectrum and that for a computed *S* spectrum amounts 68.5%, showing that the second eluent corresponds to the *S* enantiomer.

The similarity index for IR is substantially lower than the values obtained in many other studies. This deviation, most probably, is related to the appearance of a broad intense spectral feature in the experimental spectrum near 1,000 cm^{-1} , while no such band is observed in the calculated spectra. The origin of this band could not be established, but all spectroscopic data together clearly establish the (absolute) chemical structure of the compound.

8.4 | Biochemistry

The newly synthesized compound **5** (in racemic form) was screened for its inhibitory activity toward human recombinant MAO-A and MAO-B. Specific enzyme activities were calculated as 0.171 ± 0.008 nmol/(mg.min) ($n = 3$) for hMAO-A and 0.133 ± 0.009 nmol/(mg.min) ($n = 3$) for hMAO-B. The SI was expressed as K_i (MAO-A)/ K_i (MAO-B). **5** was found to inhibit hMAO-A selectively and competitively because the IC_{50} value for hMAO-A inhibition was calculated as 1.20 ± 0.02 μM , whereas the IC_{50} value for hMAO-B inhibition was calculated as 425.88 ± 16.45 μM . Its experimental SI (K_i [MAO-A]/ K_i [MAO-B]) was found to be 0.003.

For the kinetic experiments, the catalytic rates of hMAO-A and MAO-B at different p-tyramine concentrations were measured. Lineweaver-Burk graphs were constructed in the absence of the inhibitor, and in the presence of compound **5** or **5R** or **5S** and reference inhibitors. Because the lines are linear and intersect on the y-axis, compounds **5**, **5R**, and **5S** are suggested to be competitive inhibitors of hMAO-A that may interact within the catalytic site of hMAO-A. K_i values for hMAO-A and hMAO-B inhibition for **5** (racemic form) were determined as $0.91 \times 10^{-3} \pm 0.01 \times 10^{-3}$ μM and 20.00 ± 1.55 μM , respectively (Table 1). The experimental SI for **5** was found as 4.55×10^{-5} , showing that it is a remarkably selective and potent MAO-A inhibitor.

Turning to the individual isomers, isolated enantiomer **5R** inhibited both hMAO-A and hMAO-B potently. However, this compound was found to inhibit hMAO-A more potently ($K_i = 0.85 \times 10^{-3} \pm 0.05 \times 10^{-3}$ μM for hMAO-A). The experimental SI value of **5R** was found as 2.35×10^{-5} , showing that this derivative is highly selective toward hMAO-A when compared with the kinetic data of moclobemide, a known selective MAO-A inhibitor (Table 1). The kinetic behavior of **5R** is

TABLE 1 Calculated and experimental K_i values corresponding to the inhibition of hMAO isoforms by 1-[2-(2-benzoxazolinone-3-yl)acetyl]-3-phenyl-5-(3,4-dimethoxyphenyl)-4,5-dihydro-1H-pyrazole **5**

Compound	Calc. K_i Value for MAO-A (μM)	Calc. K_i Value for MAO-B (μM)	Calc. SI ^a	Exp K_i Value for MAO-A (μM) ^b	Exp K_i Value for MAO-B (μM) ^b	Exp. SI ^a	Inhibition Type, Selectivity, and Reversibility
5 (racemic)	-	-	-	$0.91 \times 10^{-3} \pm 10^{-4}$	20.00 ± 1.55	4.55×10^{-5}	MAO-A, competitive, reversible
5R	0.74×10^{-3}	29.47	2.51×10^{-5}	$0.85 \times 10^{-3} \pm 0.05 \times 10^{-3}$	36.20 ± 1.86	2.35×10^{-5}	MAO-A, competitive, reversible
5S	0.229	193.25	0.001	0.184 ± 0.007	175.00 ± 9.30	0.001	MAO-A, competitive, reversible
Selegiline (MAO-B inhibitor)	22.02	34.07	0.646	9.060 ± 0.44	0.09 ± 0.004	100.67	MAO-B, suicide inhibitor irreversible
Moclobemide (MAO-A inhibitor)	5.71	250.74	0.023	0.005 ± 0.001	1.22 ± 0.08	0.004	MAO-A, competitive, reversible

^aSelectivity index calculated as K_i (MAO-A)/ K_i (MAO-B). The selectivity toward MAO-A increases as the corresponding SI decreases, while selectivity toward MAO-B isoform increases as the corresponding SI increases.

^bEach value represents the mean \pm standard error of mean (SEM) of three independent experiments.

indicated in Figure 3. **5S** also inhibited hMAO-A and hMAO-B potently. However, the SI of **5S** was calculated as 0.001, which is poorer than that of compound **5R**. The reversibility tests were carried out using the dialysis method.⁷⁰ Compound **5** and its enantiomers **5R** and **5S** appeared as reversible inhibitors of hMAO-A (Table 2).

As seen in Table 2, moclobemide, a known selective MAO-A inhibitor, strongly inhibited hMAO-A. Following incubation of the enzyme with moclobemide, the remaining MAO-A activity was determined as $34.3 \pm 1.4\%$. hMAO-A activity was recovered up to $91.2 \pm 2.9\%$ after dialysis indicating that the inhibition is reversible. **5R**

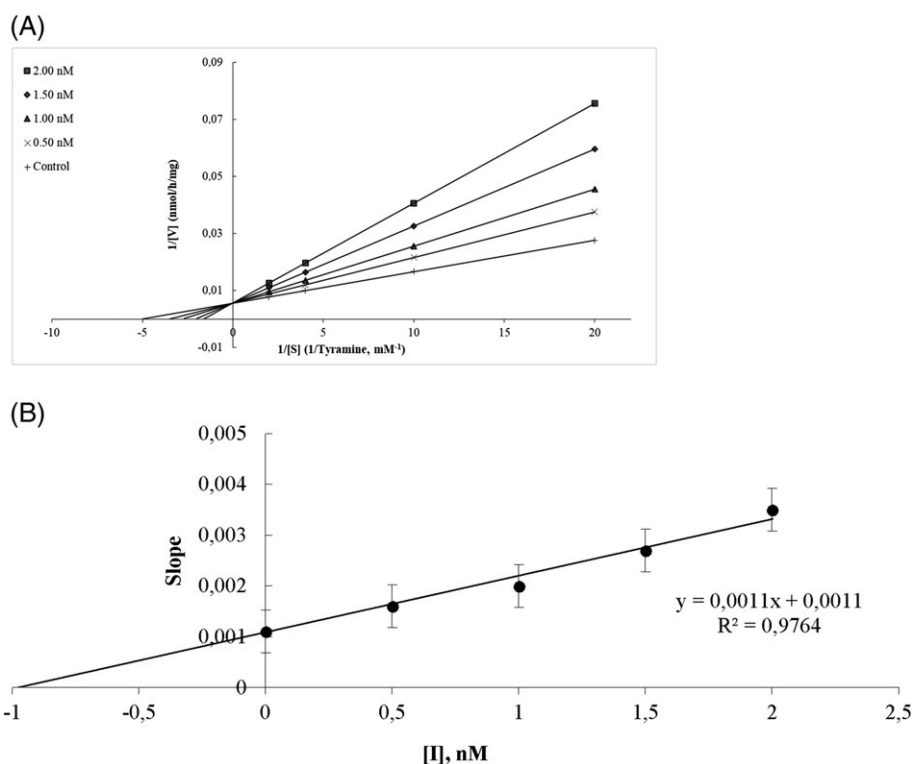


FIGURE 3 A, Lineweaver-Burk plots for the inhibition of hMAO-A by **5R**. [S]: substrate concentration (mM), [V]: reaction velocity (nmol/hour/mg). Inhibitor concentrations are shown at the left. B, The second graph represents the plots of the slopes of the Lineweaver-Burk plots versus inhibitor concentration [I]. K_i was calculated as $0.85 \times 10^{-3} \pm 0.05 \times 10^{-3}$ nM

TABLE 2 Reversibility of the inhibition of hMAOs by the novel compounds

Test Compound Incubated With hMAO	hMAO-A Activity Before Dialysis (%)	hMAO-A Activity After Dialysis (%)	hMAO-B Activity Before Dialysis (%)	hMAO-B Activity After Dialysis (%)	Reversibility
With no inhibitor	100 ± 0.00	100 ± 0.00	100 ± 0.00	100 ± 0.00	
Moclobemide	34.28 ± 1.37	91.22 ± 2.88	75.29 ± 3.01	92.00 ± 4.00	Reversible
Selegiline	91.31 ± 2.84	92.16 ± 3.14	50.29 ± 1.66	51.02 ± 2.30	Irreversible
5	39.22 ± 1.13	92.45 ± 2.34	87.26 ± 2.60	94.11 ± 3.27	Reversible
5R	10.46 ± 0.54	95.21 ± 1.33	79.50 ± 2.46	94.00 ± 2.14	Reversible
5S	30.55 ± 1.68	93.00 ± 2.11	80.60 ± 2.16	91.33 ± 2.00	Reversible

Each value represents the mean ± SEM (n = 3).

inhibited hMAO-A more potently than moclobemide (10.5 ± 0.6%). Monoamine oxidase-A activity was recovered to 95.2 ± 1.3% after dialysis, indicating that the inhibition of hMAO-A with **5R** is almost totally reversible.

In vitro cytotoxicity of the new inhibitors was tested at three different concentrations (1, 5, and 25 μM; Table 3). The results showed that they are not toxic to hepatic cells at the test concentrations.

8.5 | Molecular modeling docking studies

To rationalize the mode of interaction and the impact of the absolute configuration, molecular modeling docking studies were performed. Figure 4A to D shows the result of the molecular modeling docking of **5R** and **5S** within the MAO-A active site. Analysis of the binding modes for the **R** isomer in the MAO-A active site cavity revealed that **5R** is located in front of the FAD cofactor from re face. **5R** interacts with the active site residues lining the cavity as well as the FAD cofactor effectively (Figure 4A; $K_i = 738.93$ pM). Two hydrogen bonds occur between the side chain amine hydrogens of Lys 305 and the methoxy moieties of the phenyl group of the inhibitor. An additional hydrogen bond forms between the carbonyl groups of the inhibitor and the cofactor FAD (green dashed line in Figure 4C). In addition to these

TABLE 3 In vitro cytotoxicity of 1-[2-(2-benzoxazolinone-3-yl)acetyl]-3-phenyl-5-(3,4-dimethoxyphenyl)-4,5-dihydro-1H-pyrazole derivatives

Compound	Viability (%)		
	1 μM	5 μM	25 μM
5	95.26 ± 1.52	92.25 ± 2.01	89.26 ± 1.77
5R	97.45 ± 1.30	95.22 ± 1.85	90.22 ± 1.97
5S	93.56 ± 2.13	90.55 ± 1.03	88.77 ± 2.01

Data were expressed as mean ± SEM (n = 3). Cell viability was expressed as a percentage of the control value. $p < .05$ was considered as statistically significant.

significant interactions, four π - π interactions were identified between the side chain of Tyr407, Tyr444, and the benzoxazolinone ring of the inhibitor (pink dashed-line in Figure 4C). Also, in the 2D picture (Figure 4C), **5R** enters various Van der Waals interactions with Ile180, Asn181, Lys305, Ileu335, Phe352, Tyr69, Gln215, Tyr197, Asp339, Lys218, Ala68, Gly67, Leu337, Phe208, and Gly443 amino acids.

As shown in Figure 4B, enantiomer **5S** is located at the active site of MAO-A ($K_i = 229.44$ nM). The 2-benzoxazolinone ring cannot make effective π - π bonds with Tyr407 and Tyr444 because it cannot approach to FAD ring as in the case of **5R** isomer. The 3,4-dimethoxyphenyl ring of **5S** makes one π - σ interaction with Tyr197 and one π - π with Tyr407. The phenyl ring at position 3 of the 2-pyrazoline ring makes two π -alkyl interactions with Leu335 and Ile180 and π - π interaction with Phe208. Figure 4B and D shows that the inhibitor enters several Van der Waals interactions with Asn181, Lys305, Ileu335, Phe352, Tyr69, Gly443, and Thr408 amino acids.

The experimental data given in Table 1 agree with these observations. All of the computational inhibition results support that the MAO-A inhibitory potency of the **R** enantiomer ($K_i = 0.74 \times 10^{-3}$ μM) is much higher and 310 times more selective in comparison to the **S** enantiomer ($K_i = 0.229$ μM).

In Figure 5, **5R** and **5S** were superimposed within the MAO-A active site. As Figure 5 shows, the benzoxazolinone ring of **5R** orients itself in the hydrophobic cage surrounded by Tyr407, Tyr444, and the FAD cofactor, making four π - π interactions. In the case of **5S**, the 3,4-dimethoxyphenyl ring of the **5S** occupies the same volume of the hydrophobic cage, making only one π - σ interaction. The other moieties of the 4,5-dihydro-(1H)-pyrazole ring of both isomers do not overlap in the active site of the enzyme either. Having stereogenic center in **5** results in a very different binding mode and significant inhibition constant difference.

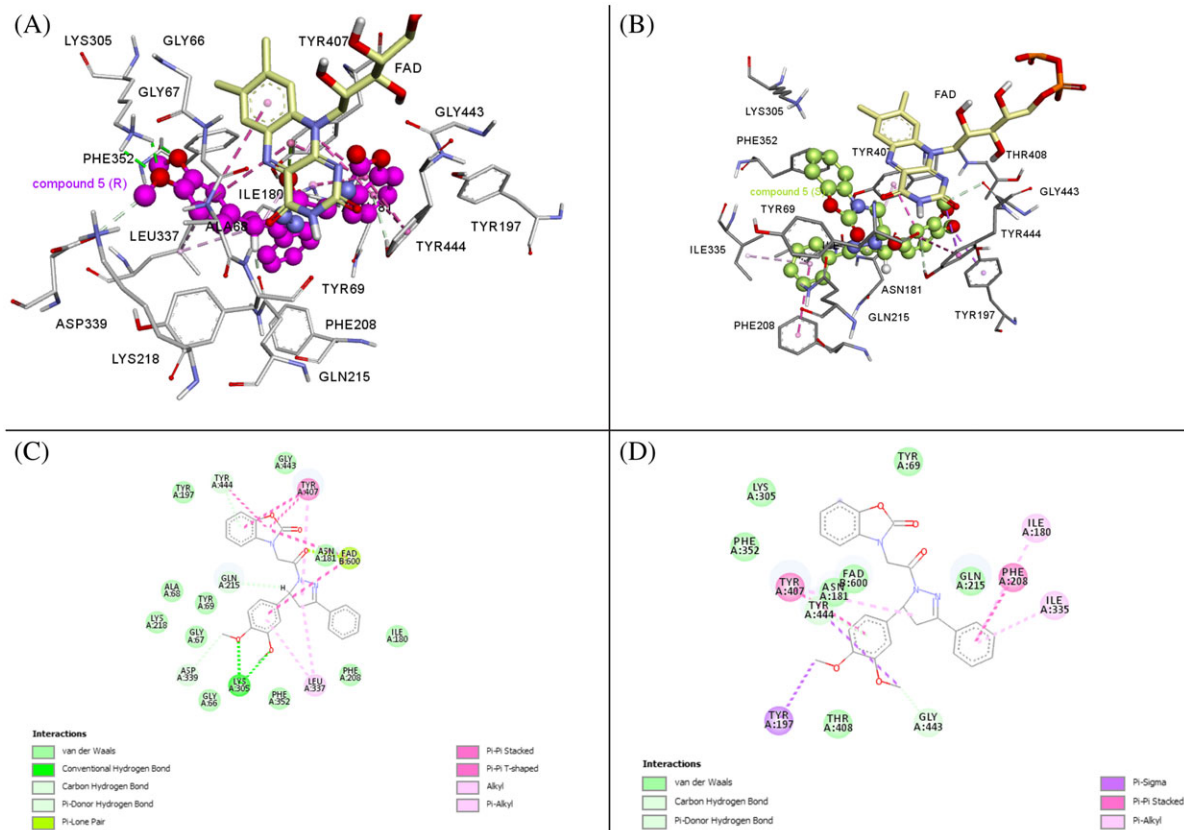


FIGURE 4 Three-dimensional representations of docked poses of the 5R isomer (A) and the 5S isomer (B) in the MAO-A active site. Two-dimensional interaction diagrams of the 5R isomer (C) and the 5S isomer (D) with amino acid residues lining the MAO-A active site

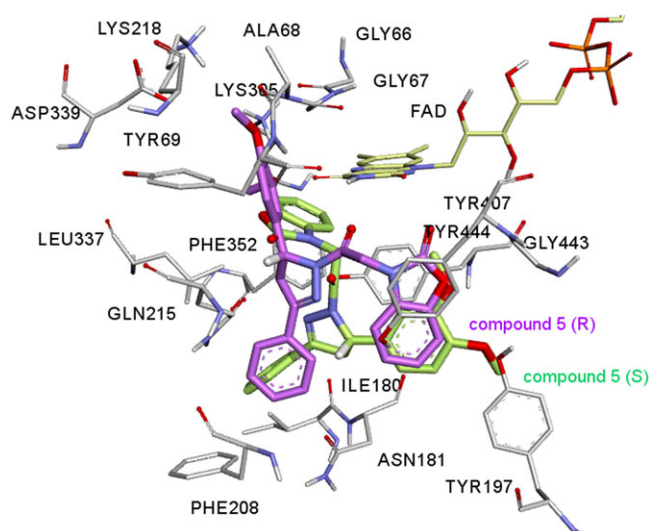


FIGURE 5 The 5R (magenta) and 5S (green) isomers superimposed within the active site of MAO-A isozyme. The hydrogen attached to the chiral C-14 are shown in white color; they are oriented differently in the active site of the enzyme

In Figure 5, 5R and 5S were superimposed within the MAO-A active site. As Figure 5 shows, the benzoxazolinone ring of 5R orients itself in the

hydrophobic cage surrounded by Tyr407, Tyr444, and the FAD cofactor, making four π - π interactions. In the case of 5S, the 3,4-dimethoxyphenyl ring of the 5S occupies the same volume of the hydrophobic cage, making only one π - σ interaction. The other moieties of the 4,5-dihydro-(1H)-pyrazole ring of both isomers do not overlap in the active site of the enzyme either. Figure 4 C and D shows the interaction diagram reflected in 2D pictures. It was seen from Figure 5 that the hydrogen attached to the chiral C-14 in 5R enantiomer forms a hydrogen bond with the Gln 215 amino acid residue; on the other hand, this interaction is absent in 5S isomer. Having stereogenic center in 5 results in a very different binding mode and significant inhibition constant difference between R and S stereoisomer.

9 | CONCLUSION

1-[2-(2-Benzoxazolinone-3-yl)acetyl]-3-phenyl-5-(3,4-dimethoxyphenyl)-4,5-dihydro-(1H)-pyrazole (5) was synthesized and separated by analytic and semipreparative HPLC technique and evaluated for in vitro inhibitory profiles of both enantiomers and the racemate toward hMAOs. Racemic 5 was found to inhibit hMAO-A

selectively and competitively. According to the expectation that the chiral center may lead to different ligand enzyme interactions, the separate enantiomers were resubmitted to in vitro biological evaluation. Isolated enantiomers **5R** and **5S** were also found to be selective MAO-A inhibitors. The experimental SI was found to be 2.35×10^{-5} for **5R**, showing that this derivative is a highly selective and potent MAO-A inhibitor compared to moclobemide. A molecular modeling docking study was carried out using PDB enzymatic models in order to evaluate the molecular interactions of the enantiomers with hMAO isoforms. **5R** appeared as the more potent and selective MAO-A inhibitor when compared to **5S**. This indicates that **5R** interacts more strongly with the active site of MAO-A than **5S**. The key factor for the efficient and selective activity is, most probably, the shorter distance between **5R** and the FAD ring at the active site of MAO.

In summary, the results show that separated enantiomers of the newly synthesized 4,5-dihydro-(1*H*)-pyrazole derivative may be promising candidates as potent MAO-A inhibitor agents. These findings may assist medicinal chemists working in this area, and in vivo studies on mice have recently been initiated.

ACKNOWLEDGMENTS

Funding by the Scientific and Technological Research Council of Turkey (project number: 112T746) and by the Hacettepe University Scientific Research Projects Coordination Unit (project number: 012D06301001 and 1527) is acknowledged. W.A.H and P.B. acknowledge support by the fund for scientific research FWO-Vlaanderen and by BOF and IOF funding schemes.

CONFLICT OF INTEREST

There are no conflicts of interest to declare.

ORCID

Nesrin Gokhan Kelekci  <http://orcid.org/0000-0001-7383-8443>

REFERENCES

- Westlund KN, Denney RM, Kochersperger LM, Rose RM. Distinct monoamine oxidase A and B populations in primate brain. *Science (Washington, D C, 1883-)*. 1985;230(4722):181-183.
- Westlund KN, Denney RM, Rose RM, Abell CW. Localization of distinct monoamine oxidase A and monoamine oxidase B cell populations in human brainstem. *Neuroscience*. 1988;25(2):439-456.
- Ramsay RR, Albrecht A. Kinetics, mechanism, and inhibition of monoamine oxidase. *J Neural Transm*. 2018. <https://doi.org/10.1007/s00702-018-1861-9>
- Bousquet P, Feldman J, Schwartz J. Central cardiovascular effects of alpha adrenergic drugs: differences between catecholamines and imidazolines. *J Pharmacol Exp Ther*. 1984;230(1):232-236.
- Grimsby J, Lan NC, Neve R, Chen K, Shih JC. Tissue distribution of human monoamine oxidase A and B mRNA. *J Neurochem*. 1990;55(4):1166-1169.
- Carradori S, Silvestri R. New frontiers in selective human MAO-B inhibitors. *J Med Chem*. 2015;58(17):6717-6732.
- Kumar B, Sheetal A, Mantha K, Kumar V. Recent developments on the structure-activity relationship studies of MAO inhibitors and their role in different neurological disorders. *RSC Adv*. 2016;6(48):42660-42683.
- Da Prada M, Kettler R, Keller HH, et al. From moclobemide to Ro 19-6327 and Ro 41-1049: the development of a new class of reversible, selective MAO-A and MAO-B inhibitors. *J Neural Transm Suppl*. 1990;29:279-292.
- Mellick GD, Buchanan DD, McCann SJ, et al. Variations in the monoamine oxidase B (MAOB) gene are associated with Parkinson's disease. *Mov Disord*. 1999;14(2):219-224.
- Drukarch B, van Muiswinkel FL. Drug treatment of Parkinson's disease time for phase II. *Biochem Pharmacol*. 2000;59(9):1023-1031.
- Carreiras MC, Marco JL. Recent approaches to novel anti-Alzheimer therapy. *Curr Pharm Des*. 2004;10(25):3167-3175.
- Riederer P, Lachenmayer L, Laux G. Clinical applications of MAO-inhibitors. *Curr Med Chem*. 2004;11(15):2033-2043.
- Guay DR. Rasagiline (TVP-1012): a new selective monoamine oxidase inhibitor for Parkinson's disease. *Am J Geriatr Pharmacother*. 2006;4(4):330-346.
- Youdim MBH, Edmondson D, Tipton KF. The therapeutic potential of monoamine oxidase inhibitors. *Nat Rev Neurosci*. 2006;7(4):295-309.
- Bortolato M, Chen K, Shih JC. Monoamine oxidase inactivation: from pathophysiology to therapeutics. *Adv Drug Deliv Rev*. 2008;60(13-14):1527-1533.
- Coutts RT, Baker GB, Danielson TJ. New developments in monoamine oxidase inhibitors. In: *Developments of drug and modern medicines part I. Drug design*. Chichester: Ellis Horwood Ltd; 1986:40-48.
- Erol Gunal S, Teke Tuncel S, Gokhan Kelekci N, et al. Asymmetric synthesis, molecular modeling and biological evaluation of 5-methyl-3-aryloxazolidine-2,4-dione enantiomers as monoamine oxidase (MAO) inhibitors. *Bioorg Chem*. 2018;77:608-618.
- Binda C, Wang J, Pisani L, et al. Structures of human monoamine oxidase B complexes with selective noncovalent inhibitors: safinamide and Coumarin analogs. *J Med Chem*. 2007;50:5848-5852.
- Itoh K, Hoshino K, Endo A, et al. Chiral inversion of RS-8359: a selective and reversible MAO-A inhibitor via oxido-reduction of keto-alcohol. *Chirality*. 2006;18(9):698-706.

20. Dar A, Khan KM, Ateeq HS, et al. Inhibition of monoamine oxidase-A activity in rat brain by synthetic hydrazines: structure-activity relationship (SAR). *J Enzyme Inhib Med Chem*. 2005;20(3):269-274.
21. Wouters J, Ooms F, Jegham S, Koenig JJ, George P, Durant F. Reversible inhibition of type B monoamine oxidase. Theoretical study of model diazo heterocyclic compounds. *Eur J Med Chem*. 1997;32:721-730.
22. Altomare C, Cellamare S, Summo L, et al. Inhibition of monoamine oxidase-B by condensed pyridazines and pyrimidines: effects of lipophilicity and structure-activity relationships. *J Med Chem*. 1998;41:3812-3820.
23. Binda C, Wang J, Li M, Hubálek F, Mattevi A, Edmondson DE. Structural and mechanistic studies of arylalkylhydrazine inhibition of human monoamine oxidases A and B. *Biochemistry*. 2008;47(20):5616-5625.
24. Parmar SS, Pandey BR, Dwivedi C, Harbison RD. Anticonvulsant activity and monoamine oxidase inhibitory properties of 1,3,5-trisubstituted pyrazolines. *J Pharm Sci*. 1974;63(7):1152-1155.
25. Soni N, Pande R, Kalsi TK, Gupta SS, Parmar JP. Inhibition of rat brain monoamine oxidase and succinic dehydrogenase by anticonvulsant pyrazolines. *Res Commun Chem Pathol Pharmacol*, 1987; 56(1): 129-132.
26. Yesilada A, Gokhan N, Ozer I, Vural K, Erol K. 5-Methyl-8-N-substituted-thiocarbamoyl-7,8-diazabicyclo[4.3.0]non-6-enes: evaluation as BSAO inhibitors and pharmacological activity screening. *Farmacoterapia*. 1996;51(12):775-780.
27. Manna F, Chimenti F, Bolasco A, et al. Inhibitory effect of 1,3,5-triphenyl-4,5-dihydro-(1H)-pyrazole derivatives on activity of amine oxidases. *J Enzym Inhib*. 1998;13(3):207-216.
28. Manna F, Chimenti F, Bolasco A, et al. Inhibition of amine oxidases activity by 1-acetyl-3,5-diphenyl-4,5-dihydro-(1H)-pyrazole derivatives. *Bioorg Med Chem Lett*. 2002;12(24):3629-3633.
29. Gokhan N, Yesilada A, Ucar G, K Erol A, Bilgin A. 1-N-substituted thiocarbamoyl-3-phenyl-5-thienyl-2-pyrazolines: synthesis and evaluation as MAO inhibitors. *Arch Pharm (Weinheim, Ger)*. 2003;336(8):362-371.
30. Chimenti F, Bolasco A, Manna F, et al. La Torre F. Synthesis and selective inhibitory activity of 1-acetyl-3,5-diphenyl-4,5-dihydro-(1H)-pyrazole derivatives against monoamine oxidase. *J Med Chem*. 2004;47(8):2071-2074.
31. Chimenti F, Maccioni E, Secci D, et al. Synthesis, molecular modeling studies, and selective inhibitory activity against monoamine oxidase of 1-thiocarbamoyl-3,5-diaryl-4,5-dihydro-(1H)-pyrazole derivatives. *J Med Chem*. 2005;48(23):7113-7122.
32. Ucar G, Gokhan N, Yesilada A, Yabanoglu S, Bilgin AA. Interaction of some 1-N-substituted thiocarbamoyl-3-phenyl-5-thienyl-2-pyrazolines with rat liver semicarbazide-sensitive amine oxidase (SSAO), Hacettepe Univ. *J Fac Pharm*. 2005;25:23-34.
33. Gokhan-Kelekci N, Yabanoglu S, Kupeli E, et al. A new therapeutic approach in Alzheimer disease: some novel pyrazole derivatives as dual MAO-B inhibitors and antiinflammatory analgesics. *Bioorg Med Chem*. 2007;15(17):5775-5786.
34. Yabanoglu S, Ucar G, Gokhan N, Salgin U, Yesilada A, Bilgin AA. Interaction of rat lung SSAO with the novel 1-N-substituted thiocarbamoyl-3-substituted phenyl-5-(2-pyrolyl)-2-pyrazoline derivatives. *J Neural Transm*. 2007;114(6):769-773.
35. Milcent R, Akhnazarian A, Lensen N. Synthesis of 1-(2-hydroxyphenyl)-2,4-imidazolidinedione derivatives through cyclic transformations of ethyl 2-oxo-3(2H)-benzoxazoleacetate derivatives. *J Heterocyclic Chem*. 1996;33(6):1829-1833.
36. Cakir B, Dag O, Yildirim E, Erol K, Sahin MF. Synthesis and anticonvulsant activity of some hydrazones of 2[(3H)-oxobenzoxazolin-3-yl-aceto]hydrazide. *J Fac Pharm Gazi Univ*. 2001;18(2):99-106.
37. Salgin-Goksen U, Gokhan-Kelekci N, Goktas O, et al. 1-Acylthiosemicarbazides, 1,2,4-triazole-5(4H)-thiones, 1,3,4-thiadiazoles and hydrazones containing 5-methyl-2-benzoxazolinones: synthesis, analgesic, anti-inflammatory and antimicrobial activities. *Bioorg Med Chem*. 2007;15(17):5738-5751.
38. Davey W, Tivey DJ. Chalcones and related compounds. IV. Addition of hydrogen cyanide to chalcones. *J Chem Soc*. 1958;1230-1236.
39. Dickinson R, Heilbron IM, Irving F. Intermolecular condensation of styryl methyl ketones. *J Chem Soc*. 1927;1888-1897.
40. Sahin ZS, Salgin-Goksen U, Gokhan-Kelekci N, Isik S. Synthesis, crystal structures and DFT studies of 1-[2-(5-methyl-2-benzoxazolinone-3-yl)acetyl]-3-phenyl-5-(3,4-dimethoxyphenyl)-4,5-dihydro-1H-pyrazole and 1-[2-(5-chloro-2-benzoxazolinone-3-yl)acetyl]-3-phenyl-5-(4-methoxyphenyl)-4,5-dihydro-1H-pyrazole. *J Mol Struct*. 2011;1006(1-3):147-158.
41. Gokhan-Kelekci N, Koyunoglu S, Yabanoglu S, et al. New pyrazoline bearing 4(3H)-quinazolinone inhibitors of monoamine oxidase: synthesis, biological evaluation, and structural determinants of MAO-A and MAO-B selectivity. *Bioorg Med Chem*. 2009;17(2):675-689.
42. Halgren TA, MMFF VII. Characterization of MMFF94, MMFF94s, and other widely available force fields for conformational energies and for intermolecular-interaction energies and geometries. *J Comput Chem*. 1999;20(7):730-748.
43. Halgren TA. Merck molecular force field. I. Basis, form, scope, parameterization, and performance of MMFF94. *J Comput Chem*. 1996;17(5 & 6):490-519.
44. Clark M, Cramer RD, Van Opdenbosch N. Validation of the general purpose Tripos 5.2 force field. *J Comput Chem*. 1989;10(8):982-1012.
45. Spartan'08. Wavefunction, Inc. *CONFLEX program*. Tokyo: Conflex Corporation; 2008.
46. Goto H, Osawa E. Corner flapping: a simple and fast algorithm for exhaustive generation of ring conformations. *J Am Chem Soc*. 1989;111(24):8950-8951.
47. Goto H, Osawa E. Viewpoint 11—approaches to the global minimum. *J MolStruct*. 1993;285:157-168.
48. Frisch MJ, Trucks GW, Schlegel HB, et al. *Gaussian 09, Revision C.01*. Wallingford CT: Gaussian, Inc; 2009.
49. Yanez M, Fraiz N, Cano E, Orallo F. Inhibitory effects of cis- and trans-resveratrol on noradrenaline and 5-hydroxytryptamine

- uptake and on monoamine oxidase activity. *Biochem Biophys Res Commun.* 2006;344(2):688-695.
50. Chimenti F, Maccioni E, Secci D, Bolasco A, Chimenti P, et al. Synthesis, stereochemical identification, and selective inhibitory activity against human monoamine oxidase-B of 2-methylcyclohexylidene-(4-arylthiazol-2-yl)hydrazones. *J Med Chem.* 2008;51(16):4874-4880.
51. Anderson MC, Hasan F, McCrodden JM, Tipton KF. Monoamine oxidase inhibitors and the cheese effect. *Neurochem Res.* 1993;18(11):1145-1149.
52. Bradford MM. A rapid and sensitive method for the quantitation of microgram quantities of protein utilizing the principle of protein-dye binding. *Anal Biochem.* 1976;72(1-2):248-254.
53. Petzer A, Pienaar A, Petzer JP. The interactions of caffeine with monoamine oxidase. *Life Sci.* 2013;93(7):283-287.
54. Mathew B, Haridas A, Uçar G, Baysal I, et al. Exploration of chlorinated thienyl chalcones: a new class of monoamine oxidase-B inhibitors. *Int J Biol Macromol.* 2016;91:680-695.
55. Wu CF, Bertorelli R, Sacconi M, Pepeu G, Consolo S. Decrease of brain acetylcholine release in aging freely-moving rats detected by microdialysis. *Neurobiol Aging.* 1988;9(4):357-361.
56. Son S-Y, Ma J, Kondou Y, et al. Structure of human monoamine oxidase A at 2.2-Å resolution: the control of opening the entry for substrates/inhibitors. *Proc Natl Acad Sci USA.* 2008;105(15):5739-5744.
57. Binda C, Wang J, Pisani L, et al. Structures of human monoamine oxidase B complexes with selective noncovalent inhibitors: safinamide and coumarin analogs. *J Med Chem.* 2007;50(23):5848-5852.
58. Mayo SL, Olafson BD, Goddard WA. DREIDING: a generic force field for molecular simulations. *J Phys Chem.* 1990;94(26):8897-8909.
59. Morris GM, Huey R, Lindstrom W, et al. AutoDock and AutoDockTools: automated docking with selective receptor flexibility. *J Comput Chem.* 2009;30(16):2785-2791.
60. Yelekci K, Karahan O, Toprakci M. Docking of novel reversible monoamine oxidase-B inhibitors: efficient prediction of ligand binding sites and estimation of inhibitors thermodynamic properties. *J Neural Transm.* 2007;114(6):725-732.
61. Akdogan ED, Erman B, Yelekci K. In silico design of novel and highly selective lysine-specific histone demethylase inhibitors. *Turk J Chem.* 2011;35(4):523-542.
62. FDA's Policy Statement for the Development of New Stereoisomeric Drugs. *Chirality.* 1992;4:338-340.
63. Triggle DJ. Stereoselectivity of drug action. *Drug Discov Today.* 1997;2(4):138-147.
64. Simonyi M. On chiral drug action. *Med Res Rev.* 1984;4(3):359-413.
65. Patel BK, Hutt AJ. Stereoselectivity in drug action and disposition: an overview. In: Reddy IK, Mehvar R, eds. *Chirality in Drug Design and Development.* Caplus; 2004:139-190.
66. Berova N, Nakanishi K, Woody RW (Eds). *Circular Dichroism: Principles and Applications.* Wiley-VCH; 2000:877.
67. Freedman TB, Cao X, Dukor RK, Nafie LA. Absolute configuration determination of chiral molecules in the solution state using vibrational circular dichroism. *Chirality.* 2003;15(9):743-758.
68. Polavarapu PL, Covington CL. Comparison of experimental and calculated chiroptical spectra for chiral molecular structure determination. *Chirality.* 2014;26:539-552.
69. Debie E, De Gussem E, Dukor RK, Herrebout W, Nafie LA, Bultinck P. A confidence level algorithm for the determination of absolute configuration using vibrational circular dichroism or Raman optical activity. *ChemPhysChem.* 2011;12(8):1542-1549.
70. Petzer JP, Petzer A. Leflunomide, a reversible monoamine oxidase inhibitor. *Cent Nerv Syst Agents Med Chem.* 2016;16(2):112-119.

How to cite this article: Goksen US, Sarigul S, Bultinck P, et al. Absolute configuration and biological profile of pyrazoline enantiomers as MAO inhibitory activity. *Chirality.* 2018;1-13. <https://doi.org/10.1002/chir.23027>